British Journal of Pharmacology
www.brjpharmacol.org

RESEARCH PAPER

Identification of key residues involved in adrenomedullin binding to the AM_1 receptor

HA Watkins[1,3]*, M Au[1,3]*, R Bobby[2], JK Archbold[1,3], N Abdul-Manan[4], JM Moore[4], MJ Middleditch[3], GM Williams[1,2,3], MA Brimble[1,2,3], AJ Dingley[1,2,3] and DL Hay[1,3]

[1]*School of Biological Sciences, University of Auckland, Auckland, New Zealand,* [2]*School of Chemical Sciences, University of Auckland, Auckland, New Zealand,* [3]*Maurice Wilkins Centre for Molecular Biodiscovery, University of Auckland, Auckland, New Zealand, and* [4]*Vertex Pharmaceuticals Inc., Cambridge, MA, USA*

Correspondence
Debbie L. Hay, School of Biological Sciences, University of Auckland, Auckland 1142, New Zealand. E-mail: dl.hay@auckland.ac.nz

*Joint first authors.

Keywords
adrenomedullin; G protein coupled receptor; GPCR; receptor binding; nuclear magnetic resonance spectroscopy; isothermal titration calorimetry; RAMP

Received
5 September 2012
Revised
11 December 2012
Accepted
7 January 2013

BACKGROUND AND PURPOSE
Adrenomedullin (AM) is a peptide hormone whose receptors are members of the class B GPCR family. They comprise a heteromer between the GPCR, the calcitonin receptor-like receptor and one of the receptor activity-modifying proteins 1–3. AM plays a significant role in angiogenesis and its antagonist fragment $AM_{22–52}$ can inhibit blood vessel and tumour growth. The mechanism by which AM interacts with its receptors is unknown.

EXPERIMENTAL APPROACH
We determined the $AM_{22–52}$ binding epitope for the AM_1 receptor extracellular domain using biophysical techniques, heteronuclear magnetic resonance spectroscopy and alanine scanning.

KEY RESULTS
Chemical shift perturbation experiments located the main binding epitope for $AM_{22–52}$ at the AM_1 receptor to the C-terminal 8 amino acids. Isothermal titration calorimetry of $AM_{22–52}$ alanine-substituted peptides indicated that Y52, G51 and I47 are essential for AM_1 receptor binding and that K46 and P49 and R44 have a smaller role to play. Characterization of these peptides at the full-length AM receptors was assessed in Cos7 cells by cAMP assay. This confirmed the essential role of Y52, G51 and I47 in binding to the AM_1 receptor, with their substitution resulting in ≥100-fold reduction in antagonist potency compared with $AM_{22–52}$. R44A, K46A, S48A and P49A $AM_{22–52}$ decreased antagonist potency by approximately 10-fold.

CONCLUSIONS AND IMPLICATIONS
This study localizes the main binding epitope of $AM_{22–52}$ to its C-terminal amino acids and distinguishes essential residues involved in this binding. This will inform the development of improved AM receptor antagonists.

Abbreviations
AM, adrenomedullin; Boc, *tert*-Butoxycarbonyl; CGRP, calcitonin gene-related peptide; CLR, calcitonin receptor-like receptor; DMF, dimethylformamide; DoDt, 3,6-dioxa-1,8-octane-dithiol; ECD, extracellular domain; Fmoc, 9-fluorenylmethyloxycarbonyl; HBTU, 2-(1*H*-benzotriazole-1-yl)-1,1,3,3-tetramethylaminium hexafluorophosphate; RAMP, receptor activity-modifying protein; TFA, trifluoroacetic acid; TIPS, triisopropylsilane

Introduction

Class B GPCRs are important drug targets, with their natural peptide ligands or mimetics being used to treat diseases, including diabetes and osteoporosis (Archbold *et al.*, 2011). Structural insights into peptide binding to these receptors gives guidance as to how the peptides could be modified and further improved for therapeutic purposes. Some class B

GPCRs require receptor activity-modifying proteins (RAMPs) for high-affinity peptide interactions. The receptors for adrenomedullin (AM) and the related peptides calcitonin gene-related peptide (CGRP) and amylin belong to this category. The AM receptors are heteromers of the calcitonin receptor-like receptor (CLR) and RAMPs 2 or 3, which form the AM_1 and AM_2 receptors respectively (Poyner *et al.*, 2002). CLR with RAMP1 makes the CGRP receptor but this also has affinity for AM.

AM is a paracrine factor and is involved in the development of the lymphatic and blood vasculature (Hinson *et al.*, 2000; Fritz-Six *et al.*, 2008; Ichikawa-Shindo *et al.*, 2008). Embryonic lethality, thin blood vessel walls and significant defects observed in the vascular systems of AM, CLR and RAMP2 knock-out mice can be explained by abnormalities in the blood and lymphatic vasculature (Caron and Smithies, 2001; Dackor *et al.*, 2006; 2007; Fritz-Six *et al.*, 2008; Ichikawa-Shindo *et al.*, 2008). Inhibition of AM activity by its antagonist fragment $AM_{22–52}$ can reduce vessel number and impede tumour growth (Ishikawa *et al.*, 2003). These data indicate that angiogenesis is induced by AM through the AM_1 receptor, and that this receptor could be an attractive target for diseases characterized by insufficient or excessive angiogenesis.

There is as yet very little information on the structure–function relationships of AM. In detergent micelles, AM exhibits negligible helical structure, although NMR analysis indicates that a helix is formed between residues 22 and 34, a finding that is corroborated by circular dichroism (CD) data (Robinson *et al.*, 2009; Perez-Castells *et al.*, 2012). Chimeras of AM with related peptides indicated that its C-terminal 9 amino acids may be in proximity to RAMP3 in the AM_2 receptor, but no similar data currently exist to indicate the specific regions of AM involved in its binding to the AM_1 receptor (Robinson *et al.*, 2009).

Like other class B GPCRs, CLR is characterized by a large N-terminal extracellular domain (ECD) and seven transmembrane helices connected by intra- and extracellular loops and an intracellular C-terminal tail. Peptide binding to class B GPCRs is widely accepted to follow the two-domain model (Parthier *et al.*, 2009). The C-terminus of the peptide binds to the large ECD through hydrophobic interactions, forming an α-helix. The receptor-activating N-terminus of the peptide can then dock into its binding pocket in the juxtamembrane region (the top of the TM and adjoining region of the extracellular loops) of the receptor. ECD crystal structures of CLR with RAMP1 and RAMP2 are now available, which reveal that despite its requirement for RAMP association, CLR shows high structural similarity to class B GPCRs, which do not require RAMPs to function (Grace *et al.*, 2007; Parthier *et al.*, 2007; Pioszak and Xu, 2008; Underwood *et al.*, 2010a,b; Drechsler *et al.*, 2011). Nevertheless, the CLR/RAMP structures do not have peptide bound and there is clear evidence that RAMPs contribute to peptide binding (Qi and Hay, 2010; Archbold *et al.*, 2011). Thus, the mode of binding of AM to its receptors remains to be determined. In this study, we sought to determine the regions of $AM_{22–52}$ that are involved in binding to the AM_1 receptor with a view to designing analogues of $AM_{22–52}$ that exhibit increased affinity for the AM_1 receptor.

Methods

Peptide synthesis

$AM_{22–52}$ and its derivatives were synthesized using 9-fluorenylmethyloxycarbonyl (Fmoc) solid-phase peptide synthesis methodologies on a Tribute peptide synthesizer (Protein Technologies, Inc., Tucson, AZ, USA). The peptides were assembled on a 0.1 mmol scale using Aminomethyl ChemMatrix resin (PCAS Biomatrix Inc., Quebec, Canada) derived with the Fmoc-RINK linker (GL-Biochem, Shanghai, China) so as to afford a C-terminal amide on cleavage from the resin.

Fmoc deprotections were carried out by twice treating the resin with 3 mL of 20% piperidine (Sigma-Aldrich, St. Louis, MO, USA) in dimethylformamide (DMF) (Scharlau, Gillman, SA, Australia) for 5 min. For each coupling, 0.5 mmol of the Nα-Fmoc-amino acid was dissolved in 2 mL of 0.23 M 2-(1*H*-benzotriazole-1-yl)-1,1,3,3-tetramethylaminium hexafluorophosphate (HBTU) (Peptides International Inc., Louisville, KY, USA) in DMF and added to the resin followed by 0.5 mL of 2 M *N*-methylmorpholine (Sigma-Aldrich) in DMF, and then allowing a reaction time of 40 min.

After its completion, the peptide was cleaved from the resin with concomitant removal of side chain-protecting groups by treatment with 10 mL of trifluoroacetic acid (TFA)/3,6-dioxa-1,8-octane-dithiol (DoDT)/H_2O/triisopropylsilane (TIPS) (94:2.5:2.5:1 v/v) for 2 h at room temperature. After filtering, the peptide was precipitated from the filtrate by adding 40 mL of ice-cold ether and then pelleted by centrifugation. The supernatant was discarded and the pellet was washed well with chilled ether, air-dried, dissolved in water (15 mL), and lyophilized and stored at –30°C in siliconized microcentrifuge tubes.

$AM_{22–52}$ labelled with ^{15}N and ^{13}C was also synthesized using Fmoc solid-phase synthesis. Labelled Fmoc-protected amino acids were purchased from Sigma-Aldrich and from Cambridge Isotope Laboratories (Andover, MA, USA). ChemMatrix aminomethyl resin was firstly derived with the Fmoc-Rink linker by treatment with a mixture composed of a 5-fold molar excess of the Fmoc-Rink acid, 5-fold molar excess of HBTU and 10-fold molar excess of diisopropylamine in DMF (acid concentration of 0.2 M). Synthesis of the peptide was carried out on a 0.025 mmol scale using this resin and a Tribute peptide synthesizer (Protein Technologies, Inc.). The iterative deprotection-coupling procedure entailed firstly treatment of the resin with 20% (v/v) solution of piperidine in DMF, washing and then incubating with approximately 0.5 mL of a solution comprising 5 equivalents of Fmoc-amino acid (0.125 mmol), 5 equivalents of 2-(6-chloro-1*H*-benzotriazole-1-yl)-1,1,3,3-tetramethylaminium hexafluorophosphate and 10 equivalents of *N*-methylmorpholine in DMF for 1 h. Upon completion of the synthesis, the final Fmoc group was removed and the peptide was cleaved from the resin over 2 h using 5 mL of a mixture of TFA, DoDt, H_2O and TIPS (94:2.5:2.5:1 v/v). The peptide was precipitated by diluting the TFA solution with 8 volumes of chilled diethyl ether, collected as a pellet by centrifugation, re-dissolved in 1:1 (v/v) acetonitrile/water and lyophilized.

Peptide purification and characterization

Unlabelled peptides were purified on a semi-preparative scale by RP-HPLC using the Dionex UltiMate® 3000 Binary Semi-preparative system (Thermo Scientific, Sunnyvale, CA, USA). Samples were purified on a Gemini C-18 column (10 × 250 mm, 5 µm, 110 Å; Phenomenex, Torrance, CA, USA) using 0.1% TFA/ultra-pure water as eluent A and 0.1% TFA/acetonitrile as eluent B and generating a linear gradient of 0–30% B over 50 min at a flow rate of 5 mL·min^{-1}. The purified material was lyophilized for 72–96 h and stored at –30°C in siliconized microcentrifuge tubes.

The identity of the purified products was confirmed by ion-spray MS on a Thermo Finnigan Surveyor MSQ Plus spectrometer (Thermo Electron Corporation, Waltham, MA, USA). Analytical RP-HPLC was performed on a Gemini C-18 column (4.6 × 250 mm, 5 µm, 110 Å; Phenomenex) on a linear gradient of 0–50% buffer B over 60 min at a flow rate of 1 mL·min^{-1}, with UV absorbance monitored at 210 nm. The integration of the HPLC chromatograms at 210 nm indicated a purity of at least 90%. Amino acid analyses were performed by the Australian Proteome Analysis Facility Ltd. For assays, peptides were dissolved in water to a concentration of 1 mM, accounting for peptide content and stored as aliquots at –30°C in siliconized microcentrifuge tubes.

Purification of labelled $AM_{22–52}$ was carried out by RP–HPLC, in which 1 mL aliquots of a 8 mg·mL^{-1} aqueous solution of the peptide was loaded onto a Jupiter Proteo 4 µm 90 Å, 10 × 250 mm column (Phenomenex) and eluted with a gradient of 1–31% buffer B over 60 min. The resulting peptide is referred to as $^{13}C/^{15}N$-$AM_{22–52}$.

Cell culture and transfection

Culture of Cos-7 cells was performed as previously described (Bailey and Hay, 2006). Cells were cultured in DMEM supplemented with 8% heat inactivated FBS and 5% (v/v) penicillin/streptomycin and kept in a 37°C humidified 95% air/5%CO_2 incubator. Cells were seeded into 96 well plates at a density of 10 000 cells per well (determined using Countess Counter™; Life Technologies, Carlsbad, CA, USA) 1 day prior to transfection. Cells were transiently transfected using polyethylenimine as described previously (Bailey and Hay, 2006) using full-length HA-tagged CLR and full-length untagged RAMP1, 2 or 3 constructs. These combinations generated human CGRP, AM_1 and AM_2 receptors respectively. This nomenclature conforms to the British Journal of Pharmacology's Guide to Receptors and Channels (Alexander *et al.*, 2011).

cAMP assays

cAMP assays were performed as previously described (Gingell *et al.*, 2010). On the day of the assay, cells were serum-deprived in 50 µL per well DMEM containing 1 mM 3-isobutyl-1-methylxanthine and 0.1% BSA for 30 min. Full-length human AM (American Peptide, Sunnyvale, CA, USA), reconstituted to 1 mM in ultra-pure water, was diluted in the same medium to give a final concentration range of 1 pM–1 µM. This material was added (25 µL per well), in the absence or presence of $AM_{22–52}$ (25 µL per well), and incubated at 37°C for 15 min. Forskolin (50 µM) (Tocris Bioscience, Bristol, UK) was included as a positive control on each plate. Pre-incubation with $AM_{22–52}$ for up to 30 min did not affect our antagonist potency estimates (data not shown). After incubation, the contents of the wells were aspirated and cAMP was extracted by adding 50 µL of lysis buffer as per the AlphaScreen protocol (PerkinElmer, Boston, MA, USA). The plates were gently shaken at room temperature for 15 min. A cAMP standard curve was generated from the kit cAMP standard (AlphaScreen cAMP assay kit; PerkinElmer) in the range of 100 pM–2.6 µM, 10 µL per well and was added to a white 384-well opti-plate (PerkinElmer). Ten microliters of each cell lysate was transferred to the plate. Five microliters of acceptor beads (1:100 dilution in lysis buffer) was added to each well, the plate was sealed and incubated in the dark for 30 min at room temperature. Five microliters of the donor bead mix (1:100 dilution of donor beads and biotinylated cAMP in the lysis buffer) was added to all wells; the plate was resealed and incubated in the dark for 6 h. The plates were read using an Envision plate reader (AlphaScreen protocol; PerkinElmer). The quantity of cAMP produced was determined from the raw data using the cAMP standard curve. A comparison of $AM_{22–52}$ (American Peptide) and in-house synthesized $AM_{22–52}$ was carried out to confirm that there was no difference between these peptides (data not shown). $^{13}C/^{15}N$-$AM_{22–52}$ was also compared and behaved equivalently to unlabelled peptide (Table 2).

Data analysis and statistical procedures for cAMP assay data

Data analysis, statistical interpretation, curve fitting and graphing were undertaken using GraphPad Prism 5 (GraphPad Software Inc., San Diego, CA, USA). The data from each concentration–response curve were fitted to a sigmoidal curve using a four-parameter logistic equation in order to calculate the maximum response (E_{max}) and the log EC_{50} values, with a Hill slope of 1, after first comparing fits by *F*-test. For calculation of antagonist potency values (pA_2), agonist concentration–response curves were fitted in the absence or presence of antagonist and analysed by global Schild analysis as previously described (Hay *et al.*, 2005). $AM_{22–52}$ is a competitive antagonist (Hay *et al.*, 2003); Schild slopes were not significantly different to one and were therefore constrained to one to derive antagonist potency estimates. Statistical analysis was carried out by one-way ANOVA followed by Dunnett's test, and the significance was accepted at $P < 0.05$. Data are presented graphically as the mean of normalized data; in each experiment, data were normalized to the maximal AM response.

Recombinant protein expression and purification

CLR (23–133) and RAMP2 (36–144) constructs were constructed as previously described (Koth *et al.*, 2010) and encoded an N-terminal hexahistidine tag and Tobacco Etch Virus cleavage site on the RAMP2 construct. Expression in *Escherichia coli* Rosetta 2 cells was carried out at 37°C with induction at OD600 nm of 0.6 for 3 h at a final concentration of isopropyl thiogalactopyranoside of 0.5 mM. Bacteria were harvested by centrifugation and inclusion bodies isolated as previously described (Koth *et al.*, 2010). Twenty milligrams of both CLR and RAMP2 inclusion bodies were added to 100 mL of 8 M urea (pH 8.0) and co-refolded against refolding buffer

[20 mM Tris–HCl (pH 8.0), 500 mM L-arginine, 1 mM EDTA, 5 mM reduced glutathione, 1 mM oxidized glutathione] for 50 h at 4°C. Arginine was removed by further dialysis (12 h, 4°C) against dialysis buffer [20 mM Tris (pH 8.0), 1 mM EDTA, 10% glycerol, 50 mM NaCl] with a further change of this buffer 12 h later. Purification by ion exchange and gel filtration chromatography was carried out as previously described (Koth *et al.*, 2010). We refer to the resulting complex as the AM_1 receptor ECD. The components of the AM_1 receptor complex were digested with trypsin (Promega, Madison, WI, USA) and then analysed by reversed-phase LC-MS/MS on a QSTAR XL (AB Sciex, Foster City, CA, USA). Matches with cloned sequences were identified using Mascot v2.0.05 software (Matrix Science, London, UK) and by manual interpretation of some spectra representing modified sequences. Peptide peak areas were integrated using the LC-MS Reconstruct tool within Analyst QS1.1 software (AB Sciex).

Analytical gel filtration

Analytical gel filtration was carried out using a Superdex 75 10/300 GL column (GE Healthcare, Buckinghamshire, UK) and low MW standards (Sigma-Aldrich) of 66, 29, 12.4 and 6.5 kDa. In addition, 0.5 mL of purified AM_1 receptor ECD, CLR and MW standards were loaded onto the column as separate runs in gel filtration buffer.

Isothermal titration calorimetry (ITC)

ITC was undertaken on a MicroCal ITC titration calorimeter (MicroCal Inc., Northampton, MA, USA). All experiments were carried out in duplicate. The reaction cell contained purified AM_1 receptor ECD in the gel filtration buffer [20 mM Tris (pH 8.0), 150 mM NaCl, 1 mM EDTA, 10% glycerol] at 30 μM, degassed at 1/3 atm for 10 min. $AM_{22–52}$ or its analogues were dissolved in the gel filtration buffer to 300 μM and similarly degassed. The peptide was titrated into the cell over 27 titrations of 10 μL at 400 s intervals. The experiment was carried out at 25°C and a stirring speed of 307 r.p.m. Heats of dilution were determined from control titrations; peptide was injected into buffer or buffer injected into AM_1 receptor under the same conditions. The heat generated per injection was obtained by numerical integration of the raw data. Heats of dilution were subtracted from the observed heats of binding before model fitting and parameter calculation. A one set of sites binding model was used, from which the dissociation constant (K_d), the enthalpy and entropy of binding (H and S, respectively) and the binding stoichiometry were calculated.

CD spectroscopy

CD measurements were carried out as previously described (Robinson *et al.*, 2009) using a π-Star 180 spectrometer (Applied Photophysics, Leatherhead, UK). CD spectra for $AM_{22–52}$ or its analogues in 50% trifluoroethanol (TFE) at 50 μM were collected from 260 to 180 nm at 1 nm intervals with a bandwidth of 1 nm and a data collection time of 1 s at each wavelength under nitrogen gas. An average of five spectra was taken and baseline data for 50% TFE alone were subtracted to give absolute CD values. Molar ellipticity values for these spectra were calculated and analysed for secondary structure content using the K2D program (Andrade *et al.*, 1993).

NMR sample preparation

NMR samples contained 0.6 mM isotope-labelled $^{13}C/^{15}N$ $AM_{22–52}$ or 0.4 mM isotope-labelled $^{13}C/^{15}N$ $AM_{22–52}$ in a 1:2 ratio with the AM_1 receptor ECD. NMR samples were prepared in 20 mM Tris–HCl (pH 6.1), 1 mM EDTA, 150 mM NaCl and 93/7% (v/v) H_2O/D_2O.

NMR spectroscopy and data processing

NMR experiments were performed at 298 K using a Bruker AV600 spectrometer (Bruker Corporation, Rheinstetten, Germany) equipped with a 5-mm z-gradient $^1H/^{15}N/^{13}C$ cryoprobe optimized for ^1H detection. All experiments were performed with the ^1H carrier positioned on the ^1H_2O resonance and the ^{15}N carrier at 117.1 p.p.m.

Two-dimensional (2D) ^1H-^{15}N HSQC experiments were recorded using conventional watergate and water flip-back methods (Grzesiek and Bax, 1993). The data matrix consisted of 128* × 1024* data points (where n* refers to complex points) with acquisition times of 72.6 (t_N) and 136.4 ms (t_{HN}). The recycle delay was 1.1 s, with eight transients per increment. The total experimental time was 20 min. ^{15}N decoupling was applied during data acquisition. ^{13}C decoupling was achieved using an adiabatic pulse placed in the centre of the t_N period. Proton chemical shifts were referenced to TSP, whereas the ^{15}N and ^{13}C chemical shifts were indirectly referenced according to the ratios given by Wishart *et al.* (1995).

The triple resonance three-dimensional (3D) spectra [CBCANH, CBCA(CO)NH, HNCA] were recorded as constant-time water flip-back experiments (Grzesiek and Bax, 1992a,b; 1993). The CBCANH and CBCA(CO)NH data matrices consisted of 70*(t_1) × 37*(t_2) × 1024*(t_3) data points, with acquisition times of 6.6, 21.7 and 136.4 ms respectively. The total acquisition time for each experiment was 16 h. The 3D HNCA data matrix consisted of 55*(t_1) × 35*(t_2) × 1024*(t_3) data points, with acquisition times of 11.4, 19.8 and 136.4 ms respectively. The total acquisition time was 48 h. The ^{13}C carrier was positioned at 53 p.p.m. in the 3D experiments. Datasets were processed using NMRPipe (Delaglio *et al.*, 1995) and analysed with CcpNmr analysis (Vranken *et al.*, 2005).

Chemical shift perturbation

For analysis of the backbone $^1H^N$ and ^{15}N chemical shift perturbations, a weighed average chemical shift change was calculated using the following equation (Grzesiek *et al.*, 1996):

$$\Delta_{ave} = \sqrt{\frac{\Delta\delta_{NH}^2 + \frac{\Delta\delta_N^2}{25}}{2}}$$

where $\Delta\delta_{NH}$ is the proton chemical shift change and $\Delta\delta_N$ is the ^{15}N chemical shift change.

Results

Isolation of the AM_1 receptor ECD

Co-refolding of CLR (23–133) and RAMP2 (36–144) into 500 mM arginine from 8 M urea proceeded with no precipi-

tate visible after 50 h of dialysis; a small amount of precipitation occurred upon removal of arginine by dialysis into the dialysis buffer. This may have been due to impurities in the inclusion body preparations. Anion exchange and gel filtration chromatography yielded a stable receptor ECD complex that co-eluted as a single peak after both chromatography processes (Figure 1A). Functional folding and complex formation of the AM_1 receptor ECD was confirmed by ITC, which gave a K_d of 5 μM for $AM_{22–52}$ (Figure 1B). The data also confirmed the presence of a single AM_1 receptor binding site for the $AM_{22–52}$ peptide. Analytical gel filtration of the AM_1 receptor ECD at a concentration of 0.5 mg·mL^{-1} revealed a single peak eluting at a volume corresponding to a MW of 46.5 kDa. The expected MW of the AM_1 receptor heterodimer is 29.4 kDa, composed of the 16.3 kDa RAMP2 and 13.1 kDa CLR molecules (Figure 1C). Protein complex digestion and LC-MS/MS followed by searching against the predicted fragments for CLR and RAMP2 using the Mascot software yielded a positive identification for the peptides. Peak integration of the LC-MS/MS data of the peptide fragments revealed a 1.5:1 ratio of CLR to RAMP2 (Figure 1C). This indicates the presence of a CLR homodimer and a RAMP2 monomer in the AM_1 receptor complex. A complex with this stoichiometry would have an expected MW of 42.5 kDa. This corresponds to a MW of 46.5 kDa observed by analytical gel filtration chromatography.

Identification of the AM_1 receptor epitope of $AM_{22–52}$

We undertook solution-state NMR studies on $^{13}C/^{15}N$ $AM_{22–52}$ to identify key residues located at the binding interface between the AM_1 receptor ECD and the peptide. The 2D ^{1}H-^{15}N HSQC spectrum of apo-$AM_{22–52}$ is presented in Figure 2A. The sequence-specific ^{1}H-^{15}N assignments of apo-$AM_{22–52}$ were derived from 3D CBCANH and CBCA(CO)NH experiments, and resonances are labelled with assignment information. Chemical shift indexing with the $^{1}H_N$, $^{1}H_\alpha$, $^{13}C_\alpha$ and $^{13}C_\beta$ chemical shifts indicated that there was no apparent secondary structure present in the apo-form of $AM_{22–52}$ (Supporting Information Figure S1, Table S2). However, a distinct linear epitope was evident at the C terminus of the peptide (Supporting Information Figure S1). The uniform incorporation of ^{13}C and ^{15}N into the synthetic $AM_{22–52}$ peptide facilitated backbone resonance assignment of $AM_{22–52}$ in complex with the AM_1 receptor ECD (Figure 2A). To achieve backbone resonance assignment of the peptide complex with the receptor, a 3D HNCA spectrum was used in conjunction with the available assignment information of the apo-peptide. Although all backbone $^{1}H^N$ and ^{15}N resonances were assigned for $AM_{22–52}$ in the free form, assignments for residues Q24, I47 and Y52 were not assigned in the peptide-receptor complex. For these residues, resonances were either not visible or significantly line-broadened in the 2D ^{1}H-^{15}N HSQC spectrum, indicative of chemical exchange broadening resulting from flexibility on the microsecond to millisecond timescale. In addition, resonances for residues Y31, Q32, F33, T34, N40, V41, A42, R44 and G51 were weak and were only observed at low contour levels (resonance frequencies are depicted as dashed circles in Figure 2A). These resonances are likely to be affected by chemical exchange, therefore leading to a reduction in signal intensity.

The 2D ^{1}H-^{15}N HSQC for $AM_{22–52}$ in complex with the AM_1 receptor ECD shows the same resonance dispersion as observed in the spectrum of the free form (Figure 2A). Significant differences in linewidths and chemical shift perturbations were observed upon complex formation. A qualitative analysis of the chemical shift perturbation was performed using the normalized weighed $^{1}H^N/^{15}N$ chemical shift average, as shown in Figure 2B, for $AM_{22–52}$ in its free and AM_1 receptor ECD bound form. The results indicate that resonances arising for residues located in the C-terminal segment of the peptide exhibit strong variations in chemical shifts between the free form and the complex. Residues with a weighed chemical shift perturbation (Δδ) larger than 0.15 p.p.m. (average plus 1 SD) are S45 (Δδ = 0.65 p.p.m.), K46 (Δδ = 0.25 p.p.m.) S48 (Δδ = 0.33 p.p.m.), Q50 (Δδ = 0.38 p.p.m.) and G51 (Δδ = 0.70 p.p.m.), with an average of 0.4620 ± 0.0403 p.p.m. over these residues (Figure 2B). Residues located in the N-terminal segment (i.e. residues 24–44) showed a significantly smaller average chemical shift perturbation (0.0170 ± 0.0004 p.p.m.), indicating that these residues are not at the key binding interface and the small changes reflect subtle conformational rearrangements being transmitted through the peptide to facilitate binding to the receptor. Unfortunately, due to missing assignment information, chemical shift perturbations could not be obtained for residues Q24, I47 and Y52. The chemical shift mapping results clearly indicate that the C-terminal segment of $AM_{22–52}$ is a major AM_1 receptor ECD binding epitope.

Alanine substitution of $AM_{22–52}$ residues 44–52

To investigate and characterize the roles of the individual amino acids constituting this major AM_1 receptor ECD binding epitope of $AM_{22–52}$, each residue in this region was individually replaced with alanine. Two complementary methods were used to determine the impact of these substitutions: binding affinities of these peptides were determined by ITC at the AM_1 receptor ECD and in functional assays at the full-length AM_1, AM_2 and CGRP receptors.

All ITC experiments were carried out at a concentration of 30 μM AM_1 receptor ECD, with a 10-fold excess of peptide. The measurements for each peptide were carried out in duplicate using a different preparation of AM_1 receptor ECD for each experiment. Y52A, G51A and I47A $AM_{22–52}$ completely abolished binding to the AM_1 receptor ECD (Table 1), indicating that these residues are intrinsically involved in $AM_{22–52}$ binding to the AM_1 receptor. K46A $AM_{22–52}$ resulted in a 10-fold decrease in binding affinity. Small changes in binding affinity were seen for Q50A, P49A, S48A and R44A $AM_{22–52}$. The chemical shift changes seen in the NMR HSQC experiments for these residues may be due to a change in their molecular environment because of their increased proximity to the AM_1 receptor ECD. This change in environment could also be due to a structural change within the peptide occurring upon its binding to the receptor.

The binding affinity of $AM_{22–52}$ at 37°C was determined in the same manner as that measured at 25°C and showed a decrease in binding affinity to 29 μM. The enthalpy change became more negative at –31.4 kcal·mol^{-1} when the experiment was conducted at 37°C, indicating that the $AM_{22–52}$-AM_1

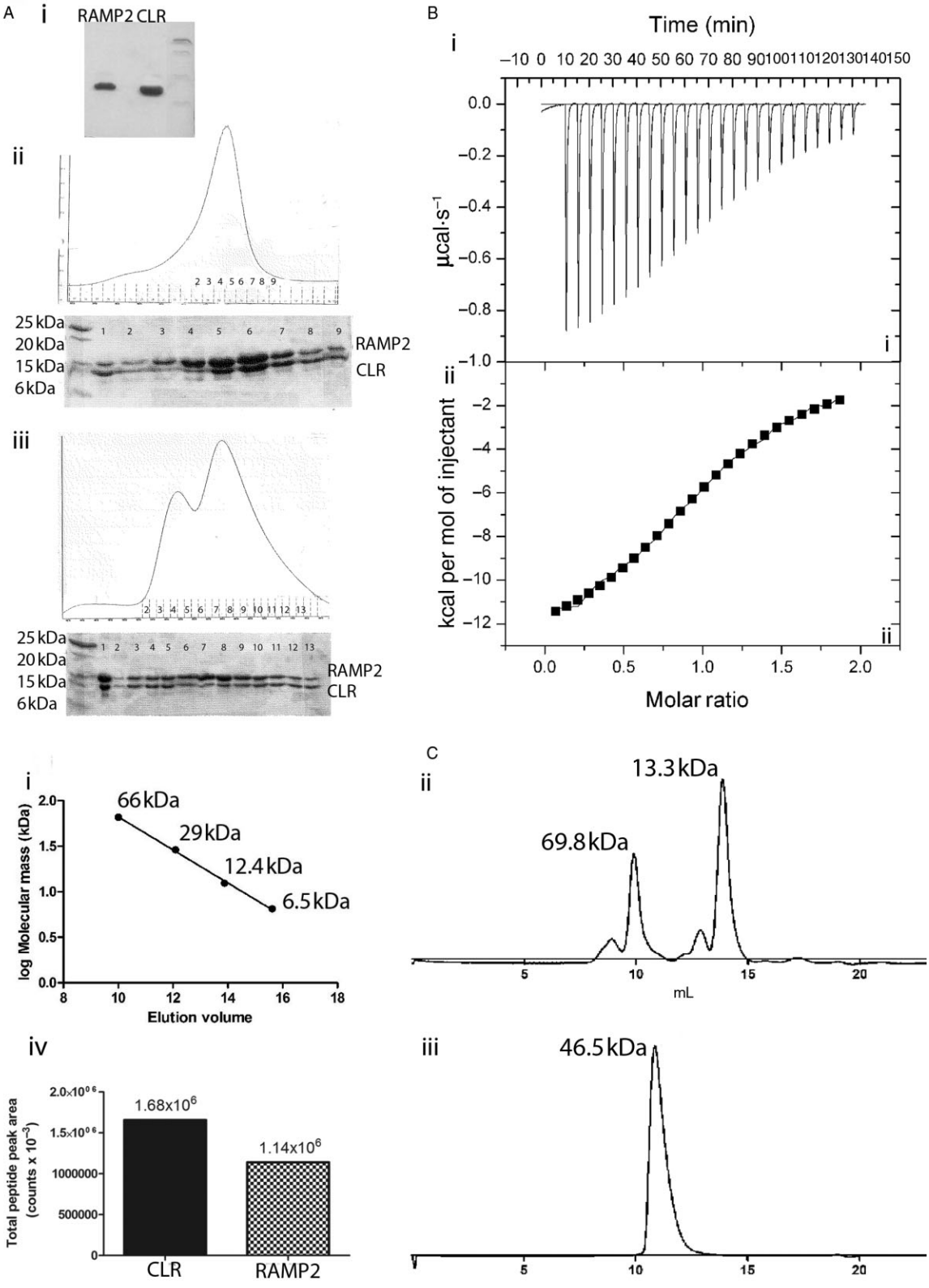
A
i
RAMP2 CLR
ii
2 3 4 5 6 7 8 9
25 kDa
20 kDa
15 kDa
6 kDa
1 2 3 4 5 6 7 8 9
RAMP2
CLR
iii
2 3 4 5 6 7 8 9 10 11 12 13
25 kDa
20 kDa
15 kDa
6 kDa
1 2 3 4 5 6 7 8 9 10 11 12 13
RAMP2
CLR
B
Time (min)
i
–10 0 10 20 30 40 50 60 70 80 90100110120130140150
0.0
−0.2
−0.4
−0.6
−0.8
−1.0
µcal·s⁻¹
i
ii
kcal per mol of injectant
−2
−4
−6
−8
−10
−12
ii
0.0 0.5 1.0 1.5 2.0
Molar ratio
C
i
66 kDa
29 kDa
12.4 kDa
6.5 kDa
log Molecular mass (kDa)
2.0
1.5
1.0
0.5
0.0
8 10 12 14 16 18
Elution volume
ii
13.3 kDa
69.8 kDa
5 10 15 20
mL
iii
46.5 kDa
5 10 15 20
iv
Total peptide peak area (counts x 10⁻³)
2.0x10⁰⁶
1.5x10⁰⁶
1000000
500000
0
1.68x10⁶
1.14x10⁶
CLR
RAMP2

Figure 1

(A) SDS-PAGE analysis from refolding and purification of $RAMP2_{36–144}$ and $CLR_{23–133}$ inclusion bodies to generate pure AM_1 receptor ECD for NMR analysis and biophysical studies. (i) Purified CLR and RAMP2 inclusion bodies in 8 M urea, 0.1 M Tris–HCl (pH 8.0). (ii) Ion-exchange chromatography trace monitoring absorbance at 280 nm and SDS-PAGE analysis of ion exchange chromatography of refolded AM_1 receptor ECD complex. The contents of each lane on the SDS-PAGE gel contain protein from the corresponding eluted fractions illustrated on the trace above. Lane 1 shows co-refolded receptor components. Fractions in lanes 2–5 contain mainly RAMP2 alone and some impurities. Lanes 6–9 contain an approximate 1:1 complex of $RAMP2_{36–144}$ and $CLR_{23–133}$ forming the AM_1 receptor; these were pooled and loaded onto a gel filtration column. (iii) Gel filtration chromatography trace monitoring absorbance at 280 nm and SDS-PAGE analysis of the AM_1 receptor ECD complex. Fractions in lanes 8–13 contain $RAMP2_{36–144}$ and $CLR_{23–133}$ in an approximate 1:1 complex which constitutes the pure AM_1 receptor ECD. These fractions were pooled and concentrated to 30 μM and used in isothermal titration calorimetry (ITC). Fractions in lanes 2–7 contain possible higher MW aggregates of the receptor complex. Lane 1 contains the crude AM_1 receptor complex from ion exchange chromatography. (B) ITC showing the (i) raw binding data for progressive 10 μL injections of $AM_{22–52}$ at 300 μM and (ii) peak integration of heats of binding. (C) Analytical gel filtration was used to confirm the size of the AM_1 receptor complex. (i) Calibration curve based on the elution volumes of four MW standards, 66, 29, 12.4 and 6.5 kDa; this was used to calculate the molecular weights corresponding to the elution peaks of the AM_1 receptor and CLR. (ii) Gel filtration chromatogram of CLR alone, a peak at 13.3 and 69.8 kDa corresponding to the monomer and a possible 5-mer aggregate were seen. (iii) Gel filtration chromatogram of the purified AM_1 receptor showing a peak at 46.5 kDa; this may correspond to a stoichiometric complex of two CLR and one RAMP2 molecule. (iv) Graph showing the summed peak areas obtained by LC-MS/MS per micromole of each protein in the digested complex. This shows a 1.5:1 CLR : RAMP2 ratio in the AM_1 receptor complex.

Table 1

Isothermal titration calorimetry for $AM_{22–52}$ and alanine analogues of the C-terminal nine residues of $AM_{22–52}$ at the AM_1 receptor ECD

Peptide	K_d (μM)	H (kcal·mol^{-1})	S (cal·K^{-1}·mol^{-1})
$AM_{22–52}$	5.00	–13.62	–21.7
Y52A $AM_{22–52}$	No binding	–	–
G51A $AM_{22–52}$	No binding	–	–
Q50A $AM_{22–52}$	7.35	–10.4	–11.4
P49A $AM_{22–52}$	12.1	–7.53	–2.73
S48A $AM_{22–52}$	8.9	–115	–15.6
I47A $AM_{22–52}$	No binding	–	–
K46A $AM_{22–52}$	51.5	–	–
S45A $AM_{22–52}$	5.3	–23	–52.8
R44A $AM_{22–52}$	14.9	–18.2	–38.9

Values shown are the mean of two values ($n = 2$); in no case does the error exceed 17% of the value indicated. No binding indicates that no value was measurable due to the low affinity of the peptide-receptor interaction. – denotes an immeasurable value due to the low affinity binding and thus inaccuracy of these measurements.

receptor ECD interaction is predominantly through hydrophobic interactions.

Affinities of alanine-substituted peptides were also determined at the full-length AM_1 receptor transfected into Cos-7 cells. $AM_{22–52}$ behaves as an antagonist of AM-stimulated cAMP production. The ability of each peptide to antagonize the receptor was compared to $AM_{22–52}$ (Table 2). Y52A, G51A and I47A $AM_{22–52}$ resulted in ≥100-fold reduction in antagonist potency compared to $AM_{22–52}$. R44A, K46A, S48A and P49A $AM_{22–52}$ decreased antagonist potency by approximately 10-fold, whereas S45A and Q50A $AM_{22–52}$ showed no significant alteration (Figure 3). A peptide comprising only the C-terminal 9 amino acids (9-mer) had no detectable affinity.

AM and thus its $AM_{22–52}$ fragment can also bind to the CGRP and AM_2 receptors. To determine if these same residues are also important for binding in the presence of a different RAMP, Cos-7 cells were transfected with CLR and RAMP1 (CGRP receptor) or CLR and RAMP3 (AM_2 receptor). Similar patterns were observed for most peptides at both receptors (Table 2). P49A $AM_{22–52}$ did not, however, lose affinity at the CGRP receptor and R44A $AM_{22–52}$ only lost affinity at the AM_1 receptor.

CD spectroscopy of $AM_{22–52}$ and its alanine analogues

CD was carried out on $AM_{22–52}$, its analogues and the isolated C-terminus in order to establish that any functional change observed was not due to a change in the intrinsic structure of the peptide upon modification. No significant change in the relative proportions of α-helix or β-sheet was observed upon the introduction of the alanine substitutions (Table 3). On the other hand, the 9-mer had no secondary structure in 50% TFE.

Discussion

The ECD of the AM_1 receptor was successfully refolded and purified from its constituent RAMP2 and CLR ECDs. Analytical gel filtration yielded a MW of 46.5 kDa for the purified receptor ECD. Together with the MS data, this value indicates a stoichiometry of two CLR molecules to one RAMP2 molecule. When refolded and purified in the absence of the RAMP2 molecule, the CLR ECD shows obvious oligomerization with elution peaks corresponding to a single CLR at 13.3 and a multimer at 69.8 kDa. Recent crystal structures of the CGRP and AM_1 receptor (ter Haar *et al.*, 2010; Kusano *et al.*, 2012) indicate that the ECD of these receptor complexes exhibit a 1:1 stoichiometry of their CLR : RAMP components. These structures were solved using shortened fragments of both CLR and RAMP1 or 2 of varying length, selected for by their propensity to crystallize. Indeed, the AM_1 receptor structure used a RAMP2 fragment significantly

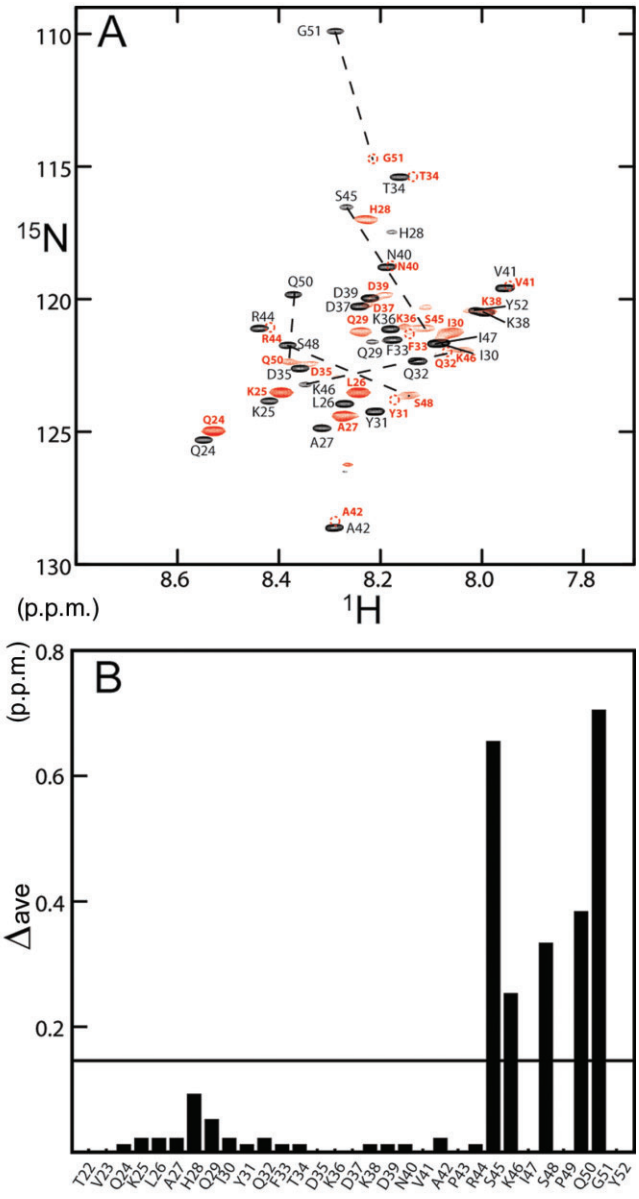

Figure 2

(A) 2D ^{1}H-^{15}N HSQC spectra of AM_{22-52} in the free-state (black) overlaid with AM_{22-52} bound to the AM_1 receptor ECD (red). Dashed circles depict resonances that were too low to be observed at the contour level plotted for the HSQC of AM_{22-52} bound to the AM_1 receptor. Residues S45, K46, S48, Q50 and G51 undergo large chemical shift perturbations. The changes in chemical shift for these resonances are indicated by black dotted lines that link the corresponding signals assigned in the free and bound states. (B) Weighted $^{1}H^{N}$, ^{15}N average chemical shifts between AM_{22-52} in the free and bound form with the AM_1 receptor ECD. The average over all residues plus 1 SD is depicted by the black line. No assignments were obtained for residues Q24, I47 and Y52 in the complex. Additionally, there are two prolines (P43, P49) in the AM_{22-52} sequence.

shorter than that used in this study. This may have selected for fragments which form a 1:1 stoichiometric complex. The asymmetric unit of the AM_1 receptor contains a dimer of the heterodimer AM_1 receptor complex in which hydrogen bonding has been observed between the two CLR molecules. It may be the case that the 46.5 kDa MW observed in analytical gel filtration in this study corresponds to a dimer of the AM_1 receptor heterodimer, as seen in the AM_1 receptor structure (Kusano *et al.*, 2012), although this would seem unlikely given the ratio of approximately 1.5:1 CLR : RAMP2 observed by MS. This non-integer ratio is most likely due to a lower molar response on average for the population of peptides representing one protein over the other; however, it nevertheless indicates a significantly higher proportion of CLR, and taken together with the apparent MW of the complex as observed by analytical gel filtration, supports a 2:1 stoichiometric ratio of CLR : RAMP2 over any other hypothesis. It is worth considering that in both crystal structures and this study, the ECD is not in its full-length physiological form and thus not subject to spatial constraints that would be present in the full-length receptors. Investigations on the oligomerization of the full-length CGRP receptor report a stoichiometry of a CLR homo-oligomer and a RAMP1 monomer, consistent with our observations for CLR and RAMP2 (Heroux *et al.*, 2007).

Irrespective of the actual stoichiometry, the purified AM_1 receptor ECD was capable of binding AM_{22-52} with a K_d of 5 μM. Binding studies of various peptide fragments to their receptors have been carried out using both ITC and surface plasmon resonance (Parthier *et al.*, 2007; Pioszak and Xu, 2008; Koth *et al.*, 2010; Drechsler *et al.*, 2011; Kusano *et al.*, 2012). Depending on the receptor and the methodology used, the binding affinities of these peptide fragments to their receptor ECDs vary across the milli- to nanomolar ranges but are predominantly in the low micromolar range. Therefore, the K_d we observed for AM_{22-52} is in-line with expectations from this literature. In the two-domain model of peptide ligand binding to this class of GPCR (Parthier *et al.*, 2009), the peptide C-terminus binds to the ECD and the peptide N-terminus binds to the receptor transmembrane bundle and extracellular loops. Thus, the affinities determined by ITC are likely to be lower when not all points of contact with the receptor are available for that particular peptide. For AM_{22-52}, the lower affinity at the ECD in ITC compared with the full-length receptor in the cAMP assay could suggest that AM_{22-52} may be making contact with parts of the receptor other than the ECD. However, differences in these assays make it difficult to directly compare values. It would be interesting to compare the affinities of different lengths of AM between the two assays.

In solution-state NMR studies, we were able to assign backbone resonances for both the apo and receptor bound forms of AM_{22-52}. Only a small number of resonances underwent large chemical shift changes when AM_{22-52} was mixed with the AM_1 receptor ECD. Nonetheless, we observed significant differences in both linewidths and chemical shift perturbations for a number of residues upon complex formation. Resonances arising from G51, Q50, S48, K46 and S45 showed a weighed chemical shift perturbation greater than the average plus 1 SD (0.15 p.p.m.), which was significantly larger than those observed for the remainder of the molecule. Assignments for I47, Y52 and Q24 were not made. These omissions notwithstanding, we can clearly locate the major AM_1 receptor ECD binding epitope of AM_{22-52} to the last eight residues at the C-terminus of the peptide.

Table 2

pA_2 values of antagonist potency for AM_{22-52} and alanine analogues of the C-terminal amino acids at full-length receptors, generated in cAMP assays

Peptide	AM_1 receptor	AM_2 receptor	CGRP receptor
AM_{22-52}	7.83 ± 0.19 (n = 6)	7.38 ± 0.10 (n = 6)	5.77 ± 0.23 (n = 6)
$^{13}C/^{15}N$ AM_{22-52}	7.88 ± 0.14 (n = 3)	ND	ND
Y52A AM_{22-52}	<4 (n = 3)[a]	<4 (n = 3)	<4 (n = 3)
G51A AM_{22-52}	<4 (n = 3)[b]	<4 (n = 4)	<4 (n = 3)
Q50A AM_{22-52}	7.45 ± 0.23 (n = 4)	6.88 ± 0.09* (n = 5)	5.81 ± 0.29 (n = 3)[c]
P49A AM_{22-52}	6.74 ± 0.10*** (n = 3)	6.53 ± 0.14*** (n = 5)	5.32 ± 0.21 (n = 3)[d]
S48A AM_{22-52}	7.03 ± 0.10** (n = 4)	6.10 ± 0.11*** (n = 4)	<5 (n = 4)
I47A AM_{22-52}	5.84 ± 0.22*** (n = 3)[c]	<5 (n = 3)	<5 (n = 3)
K46A AM_{22-52}	6.39 ± 0.17*** (n = 3)	5.96 ± 0.11*** (n = 3)	<5 (n = 3)
S45A AM_{22-52}	8.39 ± 0.09 (n = 4)	7.31 ± 0.21 (n = 4)	5.59 ± 0.20 (n = 5)
R44A AM_{22-52}	6.89 ± 0.07** (n = 3)	7.37 ± 0.18 (n = 4)	5.64 ± 0.18 (n = 4)
9-mer	<4.30 (n = 3)	<4.30 (n = 3)	<4.30 (n = 3)

Error is presented as the SEM. *P < 0.05; **P < 0.01; ***P < 0.001 versus AM_{22-52} by one-way ANOVA, followed by Dunnett's multiple comparison test.
[a]Peptide gave significant shifts in two further experiments with pA_2 values of 5.28 and 5.67 respectively.
[b]Peptide gave significant shifts in two further experiments with pA_2 values of 4.55 and 5.32 respectively.
[c]Peptide did not produce a measurable shift in the AM concentration–response curve in a further two experiments; therefore, pA_2 values could not be determined for those occasions.
[d]Peptide did not produce a measurable shift in the AM concentration–response curve in a further experiment; therefore, a pA_2 value could not be determined for that occasion.
ND, not done.

Table 3

Relative percentages of secondary structural elements for AM_{22-52} and alanine substitutions of the C-terminal nine amino acids as determined by circular dichroism spectroscopy

	AM_{22-52}	Y52A AM_{22-52}	G51A AM_{22-52}	Q50A AM_{22-52}	P49A AM_{22-52}	S48A AM_{22-52}	I47A AM_{22-52}	K46A AM_{22-52}	S45A AM_{22-52}	R44A AM_{22-52}	9-mer
α-Helix	26	28	26	23	27	26	22	28	25	27	7
β-Sheet	27	30	26	23	17	26	22	30	20	28	51
Random coil	46	42	47	53	56	47	56	42	55	45	42

Circular dichroism data were deconvoluted using the online web server K2D. These values should be used with caution; analysis using different programmes yields varying percentages and, therefore, these values are only useful for comparing between peptides and not necessarily between studies.

Guided by these NMR results and previous studies by Robinson *et al*. (2009), which implicated these amino acids of AM_{22-52} in binding to the AM_2 receptor, we made progressive alanine substitutions of the C-terminal amino acid residues of AM_{22-52}. Characterization of these peptides in ITC and functional assays further pin-pointed residues Y52, G51, I47 and K46 as essential for high-affinity receptor interactions. Each of these substitutions resulted in substantial reductions in binding affinity to the AM_1 receptor ECD and full-length receptor. CD spectroscopy indicated that there was no major structural perturbation to these peptides. This allows us to infer that these residues are present at the AM_1 receptor binding interface and may be forming discrete interactions with the receptor ECD. Previous structure–activity studies have shown that both Y52 and the C-terminal amide group characteristic of many class B GPCR peptide ligands are essential for AM binding to its full-length receptor, although they appear to have discrete roles in this process (Eguchi *et al*., 1994).

The chemical shift perturbations observed for the remaining residues in the C-terminal binding epitope determined by NMR (e.g. S45, Q50) may be due to the proximity of these residues to the binding cleft or a change in peptide structure as it binds to the receptor ECD. Thermodynamic data can give us no information on the exact nature or number of these potential interactions. The increase in negativity of the

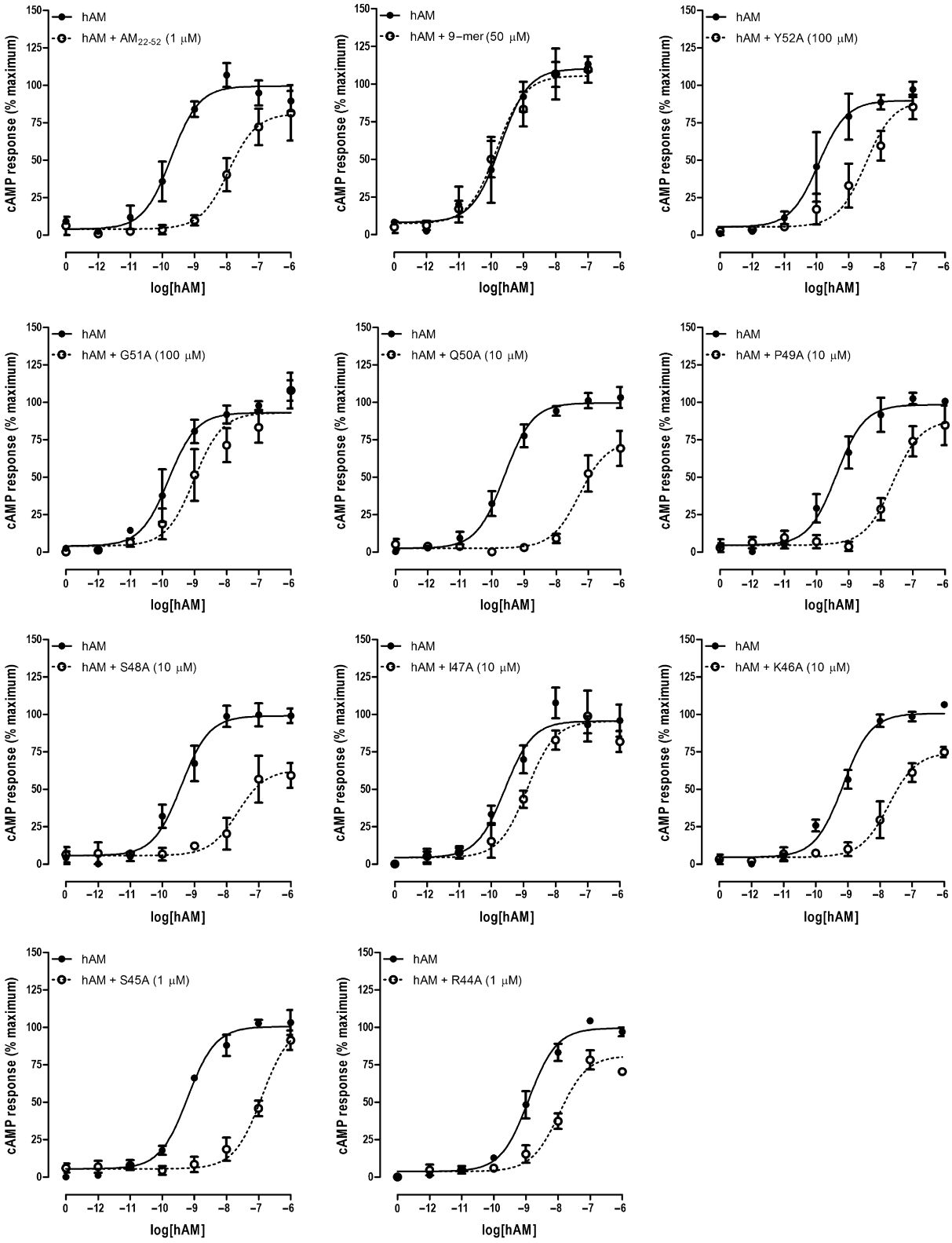

Figure 3

Concentration–response curves for the alanine mutants of $AM_{22–52}$ at the AM_1 receptor. Cos-7 cells were transfected with HA tagged CLR and untagged RAMP2 and assayed for human AM-stimulated cAMP response. Curves are plotted as a percentage of the maximal human AM-stimulated cAMP production. Each figure shows combined data from three to five independent experiments, which were each performed in triplicate. Each point on the graphs represents the mean ± SEM. Due to the different affinities of the peptides, different concentrations were used, up to the possible maximum for that peptide in order to obtain shifts.

ΔH values at 37°C compared with those at 25°C does, however, indicate that the binding interactions are of a mainly hydrophobic nature. This would be consistent with the accepted mode of binding of peptides to other class B GPCRs (Parthier *et al.*, 2009).

At the AM_2 receptor, the same residues appear to have a significant involvement in functional antagonist activity as we observed at the AM_1 receptor. Antagonist activities at the CGRP receptor were very low, meaning that any decrease in these due to the effect of alanine substitutions resulted in a complete abolition of antagonist activity detectable by our system. R44A $AM_{22–52}$ showed a selective decrease in affinity at the AM_1 receptor and also showed a threefold decrease in K_d at the AM_1 receptor ECD as determined by ITC. This may be a RAMP2-dependent residue. When it becomes possible to solve peptide bound structures of the AM_1 and AM_2 receptors, it will be interesting to see what contribution this residue makes to binding. Surprisingly, R44 did not show a substantial chemical shift perturbation when the peptide was mixed with the receptor. The reason for this discrepancy is unclear.

Interestingly, the 9-mer fragment comprising only the last nine amino acids of $AM_{22–52}$ had no measurable affinity. On the other hand, it appears unstructured in CD analysis and this may explain its lack of activity. Other portions of the peptide may be required to stabilize the conformation of this region needed for binding. Indeed, we observed small chemical shifts for the residues Q24-T34 of $AM_{22–52}$, indicating that these also have a functional role to play in the peptide (Eguchi *et al.*, 1994; Robinson *et al.*, 2009). Future studies could seek to stabilize C-terminal fragments of varying length, based on our observations of the importance of this region.

Although many crystal structures of class B GPCRs are now available, most have only short peptide fragments bound and few encompass the extreme C-terminus. The recent structure of the AM_1 receptor ECD does not have peptide bound, although it does indicate some residues in the receptor that may be involved in AM binding (Kusano *et al.*, 2012). Existing NMR structures of AM (Perez-Castells *et al.*, 2012) and $AM_{22–52}$ (Supporting Information Figure S2) are not suitable for docking into the receptor crystal structure. Those other class B GPCR structures that do include the C-terminal region of peptide fragments indicate that peptide residues involved in receptor binding are situated towards the middle of the peptide rather than at the extreme C-terminus (Parthier *et al.*, 2007; Underwood *et al.*, 2010a,b). However, alanine scanning has implicated residues closer to the C-terminus of other class B peptide ligands in receptor binding (Lang *et al.*, 2006; Grace *et al.*, 2007; Pioszak and Xu, 2008; Dong *et al.*, 2011). In particular, amino acid substitutions within a C-terminal 10-mer of CGRP showed antagonist activity in the nanomolar range (Rist *et al.*, 1998). Substitution, the enhancement of β-turns and cyclization by disulphide bond formation of this 10-mer peptide resulted in antagonists with even higher picomolar affinity for the CGRP receptor (Lang *et al.*, 2006; Yan *et al.*, 2011). Therefore, the importance of the extreme peptide C-terminus may be a particular feature of the AM and CGRP receptors. This may correlate with the requirement for RAMPs in high affinity binding; the recent structure would certainly indicate a shift in binding pocket if RAMP2 is directly involved in AM binding (Kusano *et al.*, 2012).

In this study, we have pin-pointed a discrete $AM_{22–52}$ epitope between residues R44 and Y52, which is involved in binding to the AM_1 receptor. We have defined the precise residues of $AM_{22–52}$, which are involved in binding to the AM_1 receptor and the role that they play within the binding epitope. This complements structural studies of the receptor, although more constraints are required to allow accurate docking of AM into the receptor. Our study provides useful information with which to pursue the development of high affinity antagonist analogues of $AM_{22–52}$.

Acknowledgements

The authors would like to acknowledge the following funding sources: University of Auckland, Faculty of Science Research Development Fund and the Maurice Wilkins Centre for Molecular Biodiscovery.

Conflict of interest

There are no conflicts of interest to declare.

References

Alexander SPH, Mathie A, Peters JA (2011). Guide to receptors and channels (GRAC), 5th edition. Br J Pharmacol 164 (Suppl. 1): S1–S324.

Andrade MA, Chacon P, Merelo JJ, Moran F (1993). Evaluation of secondary structure of proteins from UV circular dichroism spectra using an unsupervised learning neural network. Protein Eng 6: 383–390.

Archbold JK, Flanagan JU, Watkins HA, Gingell JJ, Hay DL (2011). Structural insights into RAMP modification of secretin family G protein-coupled receptors: implications for drug development. Trends Pharmacol Sci 32: 591–600.

Bailey RJ, Hay DL (2006). Pharmacology of the human CGRP1 receptor in Cos 7 cells. Peptides 27: 1367–1375.

Caron KM, Smithies O (2001). Extreme hydrops fetalis and cardiovascular abnormalities in mice lacking a functional adrenomedullin gene. Proc Natl Acad Sci U S A 98: 615–619.

Dackor R, Fritz-Six K, Smithies O, Caron K (2007). Receptor activity-modifying proteins 2 and 3 have distinct physiological functions from embryogenesis to old age. J Biol Chem 282: 18094–18099.

Dackor RT, Fritz-Six K, Dunworth WP, Gibbons CL, Smithies O, Caron KM (2006). Hydrops fetalis, cardiovascular defects, and embryonic lethality in mice lacking the calcitonin receptor-like receptor gene. Mol Cell Biol 26: 2511–2518.

Delaglio F, Grzesiek S, Vuister GW, Zhu G, Pfeifer J, Bax A (1995). NMRPipe: a multidimensional spectral processing system based on UNIX pipes. J Biomol NMR 6: 277–293.

Dong M, Le A, Te JA, Pinon DI, Bordner AJ, Miller LJ (2011). Importance of each residue within secretin for receptor binding and biological activity. Biochemistry 50: 2983–2993.

Drechsler N, Frobel J, Jahreis G, Gopalswamy M, Balbach J, Bosse-Doenecke E *et al.* (2011). Binding specificity of the ectodomain of the parathyroid hormone receptor. Biophys Chem 154: 66–72.

Eguchi S, Hirata Y, Iwasaki H, Sato K, Watanabe TX *et al.* (1994). Structure-activity relationship of adrenomedullin, a novel vasodilatory peptide, in cultured rat vascular smooth muscle cells. Endocrinology 135: 2454–2458.

Fritz-Six KL, Dunworth WP, Li M, Caron KM (2008). Adrenomedullin signaling is necessary for murine lymphatic vascular development. J Clin Invest 118: 40–50.

Gingell JJ, Qi T, Bailey RJ, Hay DL (2010). A key role for tryptophan 84 in receptor activity-modifying protein 1 in the amylin 1 receptor. Peptides 31: 1400–1404.

Grace CR, Perrin MH, Gulyas J, Digruccio MR, Cantle JP, Rivier JE *et al.* (2007). Structure of the N-terminal domain of a type B1 G protein-coupled receptor in complex with a peptide ligand. Proc Natl Acad Sci U S A 104: 4858–4863.

Grzesiek S, Bax A (1992a). Improved 3D triple-resonance NMR techniques applied to a 31-kDa protein. J Magn Reson 96: 432–440.

Grzesiek S, Bax A (1992b). An efficient experiment for sequential backbone assignment of medium-sized isotopically enriched proteins. J Magn Reson 99: 201–207.

Grzesiek S, Bax A (1993). The importance of not saturating water in protein NMR. Application to sensitivity enhancement and NOE measurements. J Am Chem Soc 115: 12593–12594.

Grzesiek S, Bax A, Clore GM, Gronenborn AM, Hu JS, Kaufman J *et al.* (1996). The solution structure of HIV-1 Nef reveals an unexpected fold and permits delineation of the binding surface for the SH3 domain of Hck tyrosine protein kinase. Nat Struct Biol 3: 340–345.

ter Haar E, Koth CM, Abdul-Manan N, Swenson L, Coll JT, Lippke JA *et al.* (2010). Crystal structure of the ectodomain complex of the CGRP receptor, a class-B GPCR, reveals the site of drug antagonism. Structure 18: 1083–1093.

Hay DL, Howitt SG, Conner AC, Schindler M, Smith DM, Poyner DR (2003). CL/RAMP2 and CL/RAMP3 produce pharmacologically distinct adrenomedullin receptors: a comparison of effects of adrenomedullin22-52, CGRP8-37 and BIBN4096BS. Br J Pharmacol 140: 477–486.

Hay DL, Christopoulos G, Christopoulos A, Poyner DR, Sexton PM (2005). Pharmacological discrimination of calcitonin receptor: receptor activity-modifying protein complexes. Mol Pharmacol 67: 1655–1665.

Heroux M, Hogue M, Lemieux S, Bouvier M (2007). Functional calcitonin gene-related peptide receptors are formed by the asymmetric assembly of a calcitonin receptor-like receptor homo-oligomer and a monomer of receptor activity-modifying protein-1. J Biol Chem 282: 31610–31620.

Hinson JP, Kapas S, Smith DM (2000). Adrenomedullin, a multifunctional regulatory peptide. Endocr Rev 21: 138–167.

Ichikawa-Shindo Y, Sakurai T, Kamiyoshi A, Kawate H, Iinuma N, Yoshizawa T *et al.* (2008). The GPCR modulator protein RAMP2 is essential for angiogenesis and vascular integrity. J Clin Invest 118: 29–39.

Ishikawa T, Chen J, Wang J, Okada F, Sugiyama T, Kobayashi T *et al.* (2003). Adrenomedullin antagonist suppresses *in vivo* growth of human pancreatic cancer cells in SCID mice by suppressing angiogenesis. Oncogene 22: 1238–1242.

Koth CM, Abdul-Manan N, Lepre CA, Connolly PJ, Yoo S, Mohanty AK *et al.* (2010). Refolding and characterization of a soluble ectodomain complex of the calcitonin gene-related peptide receptor. Biochemistry 49: 1862–1872.

Kusano S, Kukimoto-Niino M, Hino N, Ohsawa N, Okuda K, Sakamoto K *et al.* (2012). Structural basis for extracellular interactions between calcitonin receptor-like receptor and receptor activity-modifying protein 2 for adrenomedullin-specific binding. Protein Sci 21: 199–210.

Lang M, De Pol S, Baldauf C, Hofmann HJ, Reiser O, Beck-Sickinger AG (2006). Identification of the key residue of calcitonin gene related peptide (CGRP) 27–37 to obtain antagonists with picomolar affinity at the CGRP receptor. J Med Chem 49: 616–624.

Parthier C, Kleinschmidt M, Neumann P, Rudolph R, Manhart S, Schlenzig D *et al.* (2007). Crystal structure of the incretin-bound extracellular domain of a G protein-coupled receptor. Proc Natl Acad Sci U S A 104: 13942–13947.

Parthier C, Reedtz-Runge S, Rudolph R, Stubbs MT (2009). Passing the baton in class B GPCRs: peptide hormone activation via helix induction? Trends Biochem Sci 34: 303–310.

Perez-Castells J, Martin-Santamaria S, Nieto L, Ramos A, Martinez A, Pascual-Teresa B *et al.* (2012). Structure of micelle-bound adrenomedullin: a first step toward the analysis of its interactions with receptors and small molecules. Biopolymers 97: 45–53.

Pioszak AA, Xu HE (2008). Molecular recognition of parathyroid hormone by its G protein-coupled receptor. Proc Natl Acad Sci U S A 105: 5034–5039.

Poyner DR, Sexton PM, Marshall I, Smith DM, Quirion R, Born W *et al.* (2002). International Union of Pharmacology. XXXII. The mammalian calcitonin gene-related peptides, adrenomedullin, amylin, and calcitonin receptors. Pharmacol Rev 54: 233–246.

Qi T, Hay DL (2010). Structure-function relationships of the N-terminus of receptor activity-modifying proteins. Br J Pharmacol 159: 1059–1068.

Rist B, Entzeroth M, Beck-Sickinger AG (1998). From micromolar to nanomolar affinity: a systematic approach to identify the binding site of CGRP at the human calcitonin gene-related peptide 1 receptor. J Med Chem 41: 117–123.

Robinson SD, Aitken JF, Bailey RJ, Poyner DR, Hay DL (2009). Novel peptide antagonists of adrenomedullin and calcitonin gene-related peptide receptors: identification, pharmacological characterization, and interactions with position 74 in receptor activity-modifying protein 1/3. J Pharmacol Exp Ther 331: 513–521.

Underwood CR, Garibay P, Knudsen LB, Hastrup S, Peters GH, Rudolph R *et al.* (2010a). Crystal structure of glucagon-like peptide-1 in complex with the extracellular domain of the glucagon-like peptide-1 receptor. J Biol Chem 285: 723–730.

Underwood CR, Parthier C, Reedtz-Runge S (2010b). Structural basis for ligand recognition of incretin receptors. Vitam Horm 84: 251–278.

Vranken WF, Boucher W, Stevens TJ, Fogh RH, Pajon A, Llinas M *et al.* (2005). The CCPN data model for NMR spectroscopy: development of a software pipeline. Proteins 59: 687–696.

Wishart DS, Bigam CG, Yao J, Abildgaard F, Dyson HJ, Oldfield E *et al.* (1995). 1H, 13C and 15N chemical shift referencing in biomolecular NMR. J Biomol NMR 6: 135–140.

Yan LZ, Johnson KW, Rothstein E, Flora D, Edwards P, Li B *et al.* (2011). Discovery of potent, cyclic calcitonin gene-related peptide receptor antagonists. J Pept Sci 17: 383–386.

Supporting information

Additional Supporting Information may be found in the online version of this article at the publisher's web-site:

Figure S1 Stereo view representation of the 15 lowest energy solution structures of the $AM_{22–52}$ peptide. The amino terminus is show in dark blue, whereas the carboxy terminus is on the opposite side and shown in brown/green.

Figure S2 Overview of AM structures for residues 22–52 in solution (left) and in the presence of SDS micelles (right). Residues with elevated values from the chemical shift mapping are coloured in red (S45, K46, S48, Q50, G51).

Table S1 NMR data acquired on $AM_{22–52}$.

Table S2 Assignment and structural statistics for the 15 lowest energy structures of $AM_{22–52}$.